ACS OMEGA

Open Access

http://pubs.acs.org/journal/acsodf

Article

Room-Temperature Deposition of δ-Ni_5Ga_3 Thin Films and Nanoparticles via Magnetron Sputtering

Filippo Romeggio,* Rasmus Bischoff,# Clara B. Møller,# Victor L. Jensen,# Esteban Gioria, Rikke Egeberg Tankard, Rasmus S. Nielsen, Ole Hansen, Ib Chorkendorff, Jakob Kibsgaard, and Christian D. Damsgaard*

Cite This: *ACS Omega* 2024, 9, 49759−49766

Read Online

ACCESS | Metrics & More | Article Recommendations | Supporting Information

ABSTRACT: Magnetron sputtering is a versatile method for investigating model system catalysts thanks to its simplicity, reproducibility, and chemical-free synthesis process. It has recently emerged as a promising technique for synthesizing δ-Ni_5Ga_3 thin films. Physically deposited thin films have significant potential to clarify certain aspects of catalysts by eliminating parameters such as particle size dependence, metal−support interactions, and the presence of surface ligands. In this work, we demonstrate the potential of magnetron sputtering for the synthesis and analysis of thin film catalysts, using Ni_5Ga_3 as a model system. Initially, deposition conditions were optimized by varying the deposition pressure, followed by an investigation of the temperature effects, aiming to map a structure zone dependence on temperature and pressure as in the Thornton model. The evolution of film crystallinity was monitored using a combination of grazing incidence X-ray diffraction (GI-XRD) and high-resolution scanning electron microscopy (HR-SEM). Additionally, ultrathin films were synthesized and annealed in H_2 at high temperatures to demonstrate the possibility of producing size-controlled nanoparticles by adjusting the annealing conditions. This work demonstrates the full potential of magnetron sputtering as a technique for synthesizing model system catalysts in various forms, opening new avenues for the research and development of additional catalytic systems.

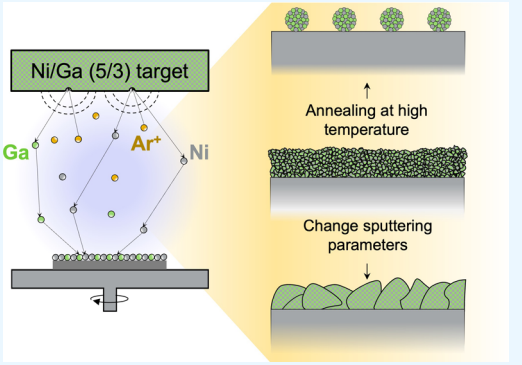

INTRODUCTION

Catalysis research faces a variety of experimental and theoretical challenges due to the complex nature of catalytic systems and their subtle behavior during reactions. Exploring novel materials for catalysis involves navigating through a multitude of adjustable parameters to probe various aspects of the system. Frequently, newly developed catalysts are swiftly synthesized through industrially relevant methods, utilizing complex chemical procedures that promise high synthesis yields and subsequent high catalyst loading. However, these methods, while mimicking potential scale-up scenarios, often lack precise control over the synthesized material, posing significant challenges in the interpretation of the results.

Especially in the context of emerging technologies, conducting systematic investigations proves highly advantageous, wherein incremental alterations to only a select few parameters facilitate a deeper comprehension of the system's fundamentals. Initially, studies may prioritize aspects such as synthesis protocols, catalytic performance, or *operando* techniques. Through methodical optimization of these individual components and a refined understanding of the catalyst's behavior, attention can then pivot toward elucidating synergistic relationships among them. This progression may entail the incorporation of more sophisticated synthesis techniques or characterization methodologies, ultimately culminating in the scaling-up of the catalytic system.

The Ni/Ga system, initially explored by Studt et al. in 2014,[1] demonstrated promising potential for the hydrogenation of CO_2 and attracted substantial of attention in the catalysis community (Figure S1). Specifically, the Ni_5Ga_3 δ-phase showed promising results with high activity and selectivity toward methanol.[1−4] The limited number of papers published to date have delved into various aspects of the catalyst, offering valuable insights for the understanding of this system. Unfortunately, none of these papers have conducted an extensive examination of the material synthesis process, but mainly focused on trying to get the best catalytic performance. Given the multitude of thermodynamically stable crystal phases within the Ni/Ga system (Figure S2), achieving the desired Ni_5Ga_3 δ-phase can prove exceptionally challenging. Therefore, there is an increasing need for an in-depth study

Received: September 12, 2024
Revised: November 29, 2024
Accepted: December 2, 2024
Published: December 9, 2024

dedicated to benchmarking the various synthesis methods and showing the expected crystallinity features of the material. In a recent study, magnetron sputtering was showed to be an effective method for obtaining pure crystal phases of the desired material. The catalyst was synthesized at lower temperatures compared to literature, evidencing a pure δ-phase,[5] on the contrary to what is usually obtained with other synthesis methods.[2] Magnetron sputtering proved to be an interesting alternative to chemical methods, resulting in the synthesis of well-defined δ-Ni_5Ga_3 at considerably lower temperatures. Nevertheless, given the different focus of that study, the technique was not deeply investigated, leaving big room for synthesis improvement.

This paper presents a comprehensive exploration of the magnetron sputtering synthesis process for Ni_5Ga_3. Initially, thin films were synthesized, building upon prior work,[5] followed by an optimization aimed at enhancing material crystallinity through adjustments to various parameters within the magnetron chamber. Building on the insights gained from thin film synthesis, the study delved deeper into magnetron sputtering as a technique for catalyst synthesis. This led to the successful synthesis of Ni_5Ga_3 nanoparticles. Figure S3a shows a summary schematics of the concept behind the study and the characterization techniques that were utilized in this study.

EXPERIMENTAL SECTION

Thin Films Preparation. The thin films were deposited on rectangular Si/SiO_2 chips (5 mm × 15 mm) consisting of a Si single crystal with a 50 nm thermally grown SiO_2 layer. The substrates were cleaned with ethanol and dried with a CO_2 blower to remove surface contaminants. Immediately after, they were placed in a magnetron sputtering system with a base pressure in the low 10^{-7} mTorr range. The samples were initially plasma-cleaned at 30 W RF power in 3 mTorr of Ar for 2 min. Subsequently, 0.3−50 nm layers of δ-Ni_5Ga_3 were deposited using DC sputtering of a bimetallic target (Ni/Ga = 62.5/37.5 At%, 99.9+% purity, purchased from Kurt J. Lesker Company) at 20 W. The samples were rotated throughout the deposition to ensure uniform coverage. The thickness was confirmed with cross-section SEM images (Figure S4). More information regarding the deposition can be found in our previous studies[5,24] and in the Supporting Information.

X-ray Diffraction. Grazing-incidence X-ray diffraction (GI-XRD) experiments were conducted using a Panalytical Empyrean X-ray Diffractometer equipped with a Cu X-ray source operating at 45 kV and 40 mA. The incident optics included a 1/32 divergence slit, a parallel beam mirror optimized for Cu X-rays, a 0.04 rad Soller slit, and a 4 mm mask. Reflected optics comprised a parallel plate collimator, a 0.04 rad Soller slit, and a Panalytical PIXcel3D detector in an open configuration. The measurements were performed at an incident angle of 0.550 ω.

X-ray Photoelectron Spectroscopy. After depositing the films in the magnetron sputtering chamber, the high vacuum conditions were broken, and the samples were transferred to a Theta Probe X-ray Photoelectron Spectrometer from Thermo Scientific. The surface composition was analyzed by XPS using a monochromatic Al K-α X-ray source (1486.68 eV). The XPS spot size was set to 400 μm, the pass energy to 50 eV, and the step size to 0.1 eV. For each core level, 50 scans were averaged. Data analysis and peak fitting were conducted using Avantage software. The survey spectrum for all deposition pressures and details of the Ni and Ga peak fittings are provided in the Supporting Information.

Scanning Electron Microscopy. The surface of the films was examined using scanning electron microscopy (SEM) with a Thermo Scientific Helios 5 Hydra UX PFIB microscope or a Helios NanoLab 600. Both the microscopes operated at an acceleration voltage of 5 kV and a beam current of 0.20 nA. The imaging was performed at a working distance of 4 mm using a Secondary Electron Through the Lens Detector (TLD) in immersion mode. These conditions were chosen to capture high-resolution images detailing the morphology and composition of the films/NPs surface.

Atomic Force Microscopy. Tapping-mode AFM measurements were carried out using a Bruker Dimension Icon AFM using a Tap150Al-G silicon tip with resonant frequency 150 kHz and a force constant of 5 N/m. The mean particle heights (Zmean) were extracted from the images using grain analysis in Gwyddion, with grains marked using Otsu's method.

RESULTS AND DISCUSSION

During magnetron sputtering, atoms are ejected from a metallic target with energies between 5 to 10 eV. When these atoms reach the substrate, their final energy varies based on the chamber's deposition conditions. This variation in energy affects the microstructure and crystallinity of the final film, significantly influencing its properties and suitability for various applications. Starting in 1973, Thornton published a series of papers on the principles of sputtering[25−28] providing an extensive guideline on the relationship between deposition temperature and pressure during film growth, yielding to the schematics shown in Figure S3b. The Thornton model describes how deposition parameters, particularly pressure and substrate temperature, influence the microstructural development of sputtered films. This model identifies four distinct zones. In Zone 1, at lower temperatures and pressures, the film growth is primarily controlled by shadowing effects rather than by atomic diffusion, resulting in a structure composed of small-diameter fibers with porous grain boundaries, as neither bulk nor surface diffusion significantly affects the growth. As deposition conditions shift into the Transition Zone (Zone T), surface diffusion begins to influence the film microstructure, particularly near the substrate where fine crystalline, V-shaped grains form. The structure becomes increasingly columnar toward the film's outer surface. While grain boundary migration remains limited, surface diffusion increases, leading to more densely packed columns. In Zone 2, a further increase in substrate temperature allows surface diffusion to become the primary growth mechanism, producing a more homogeneous grain structure across the film thickness. Grain boundary migration is now more active, resulting in larger, denser columns with enhanced crystallinity throughout the film. Finally, in Zone 3, at the highest temperatures, bulk diffusion dominates the growth process, producing films with equiaxed, three-dimensional grains and a fully dense structure characterized by substantial grain growth in all directions.

Inspired by this model, we deposited a series of Ni_5Ga_3 thin films by systematically varying the pressure and temperature. Our aim was to produce larger, well-defined crystals of the desired phase without the need for postdeposition treatment. To minimize the number of variable parameters, we maintained a constant deposition power of 20 W, following our previous study.[5] The low deposition power of 20 W was

https://doi.org/10.1021/acsomega.4c08405
ACS Omega 2024, 9, 49759−49766

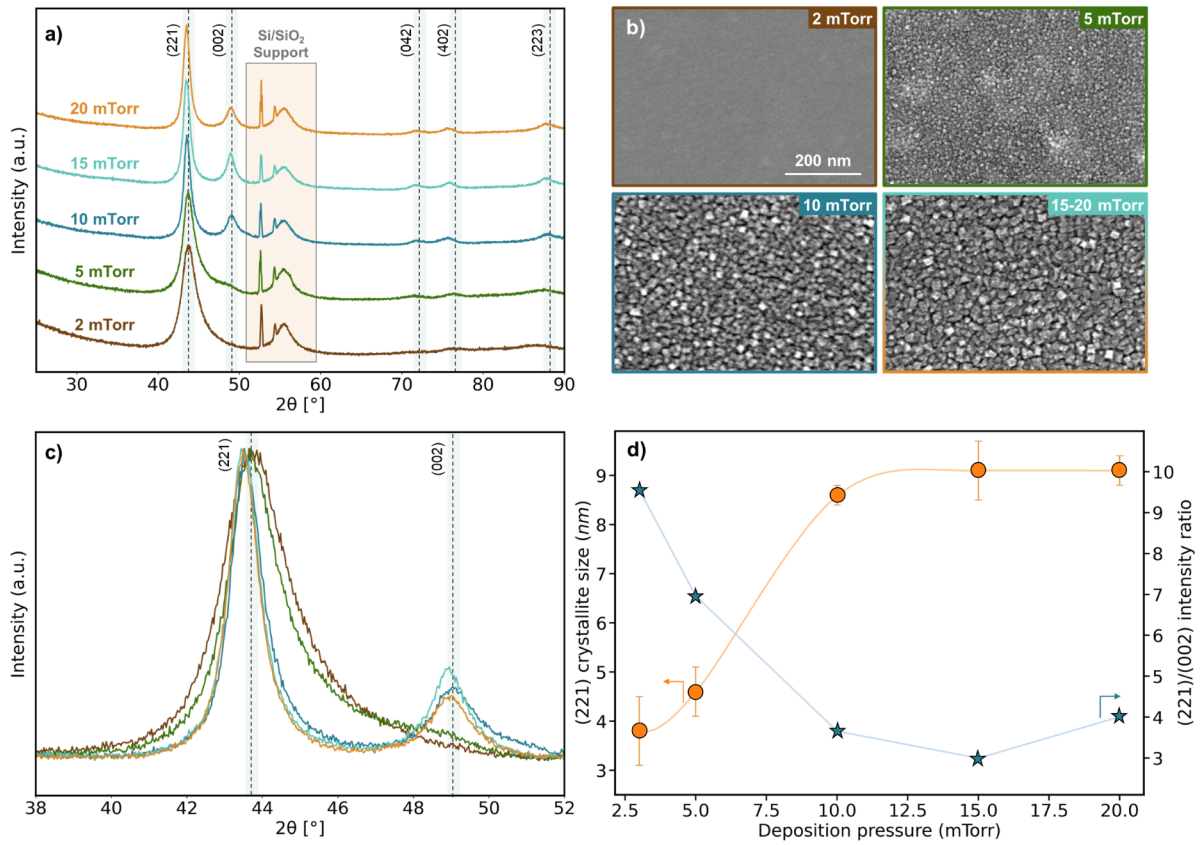

Figure 1. Pressure influence on the crystallinity of magnetron sputtered Ni_5Ga_3thin films at room temperature. (a) XRD curves (ICSD Coll. Code 103861) of thin films deposited at pressures ranging from 2 mTorr to 20 mTorr and (b) their corresponding SEM images. The targeted film thickness was 50 nm. The scale bar is the same in all SEM micrographs. (c) Zoom-in in the (221)/(002) peak region. The peaks were normalized to the (221) intensity. (d) Evolution of grain size and preferential peak growth of (002) vs (221). The crystallite size was estimated by using the Scherrer equation on the (221) peak (see Section S2.2).

selected to carefully control the deposition rate and promote the stability of the δ-Ni_5Ga_3 phase. Higher power settings typically used for Ni metal deposition (100−300 W) would lead to faster deposition rates, potentially losing the control over the deposition. Using 20 W ensures a lower energy transfer to the substrate, minimizing stress and reducing unintended heating during deposition. Figure 1a shows how the crystallinity of films changes when deposited at pressures ranging from 2 to 20 mTorr. The general trend observes an increase in crystal grain size with pressures (potentially going from Zone T to Zone 1, as shown in Figure S3b). At 5 mTorr, the (002) peak emerges around 49 degrees, becoming more prominent at pressures above 10 mTorr along with other orientations at higher diffraction angles. While the (221) peak confirms the sample crystallinity even at low pressures deposition, the presence and intensity of the (002) peak provide additional insight into the film's preferred orientation and structural ordering.

To confirm the trend observed in the XRD results, SEM images were taken for each film. Figure 1b confirms that the grains increase in size with pressure, especially when going from 5 to 10 mTorr, after which a growth plateau is reached. These findings demonstrate that magnetron sputtering can effectively synthesize the desired δ-phase of Ni_5Ga_3 without the need of any substrate heating nor postdeposition annealing. This result is particularly noteworthy when compared to chemical methods reported in the literature (Table 1), which require harsher conditions for the synthesis of the δ-phase.

Table 1. Literature Overview on Ni_5Ga_3 Synthesis Conditions[abc]

Method	Synthesis condition	Reference	Year[c]
IWI	>600 °C in H_2	[1−3,6−15]	2014
CP	>600 °C in H_2	13,[16−20]	2017
Co-condensation-evaporation	500 °C calcination + $NaBH_4$ in ethanol	[8, 9,13, 21]	2017
Metal melting	melting at 1500 °C	9	2019
Urea hydrolysis	700 °C in H_2	11	2020
Inverse micelle encapsulation	470 °C calcination + 700 °C in H_2	22	2022
Co-grafting	600 °C in H_2	4	2024
Ball milling	500 °C calcination + 600/700 °C in H_2	23	2024
Magnetron Sputtering	385 °C in H_2	5	2024
Magnetron Sputtering	**Room temperature**	**This work**	**2024**

[a]Summary of all the manuscripts published on Ni_5Ga_3 for CO_2 to methanol and their synthesis conditions to form the desired δ-phase. [b]IWI = Incipient Wetness Impregnation, CP = Co-Precipitation. [c]Only the year of the first publication for each method is reported.

When comparing these results to the previous study,[5] it is clear that adjusting just one deposition parameter can significantly influence the films. This underscores the importance of optimizing the synthesis parameters by fully exploiting the potential of magnetron sputtering.

https://doi.org/10.1021/acsomega.4c08405
ACS Omega 2024, 9, 49759−49766

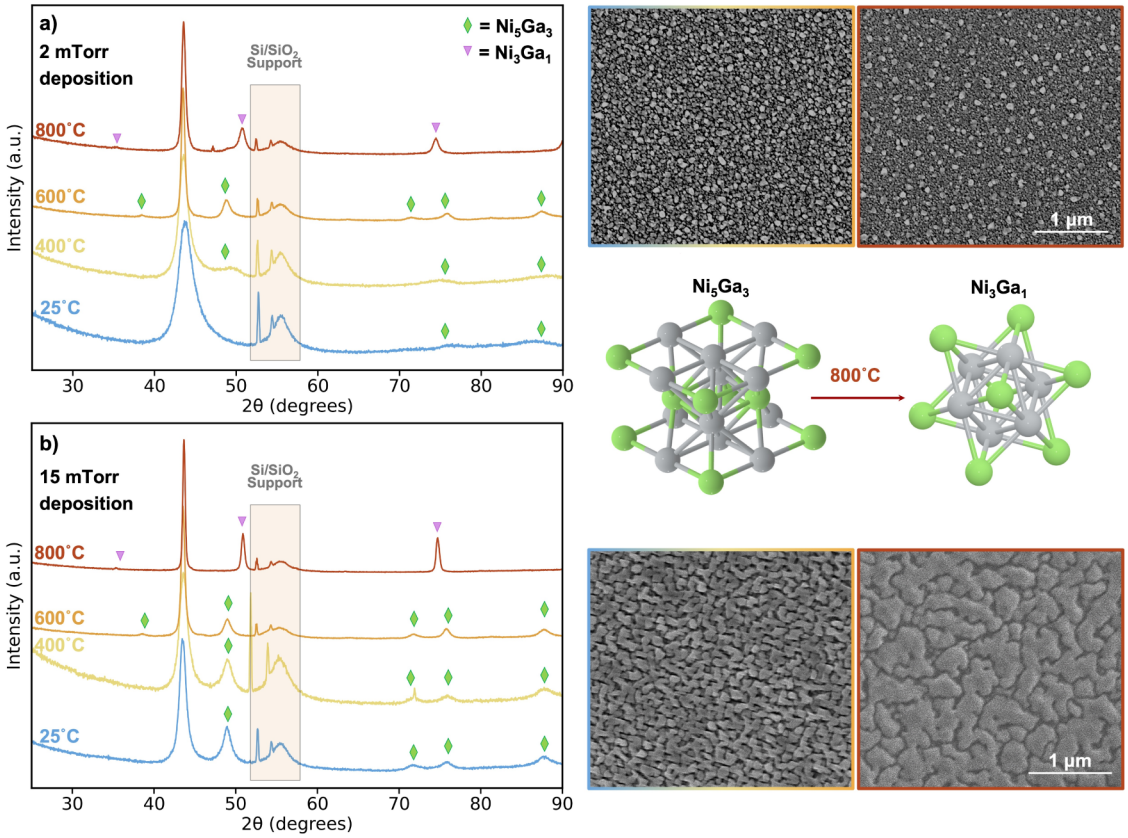

Figure 2. Temperature influence on the crystallinity of magnetron sputtered Ni_5Ga_3thin films. (b) XRD curves of thin films deposited at 2 mTorr and 15 mTorr. On the right, their corresponding SEM images of the thin films annealed at 600 and 800 °C. The targeted film thickness was 50 nm. The scale bar is the same in all SEM micrographs.

The observed increase in the crystal grains size with pressure is more pronounced than predicted by the model in Figure S3b, suggesting that the deposition pressure has a more significant influence on the process. One way to conceptualize this is by imagining the magnetron chamber as the condensation chamber of a cluster source, where argon acts as a third collision body, allowing nanoparticles to form in-flight before reaching the substrate. In this context, the Ar atoms play a critical role in ensuring the conservation of both energy and momentum, thereby stabilizing the emerging dimers.[29−31] These can subsequently act as a nucleation site, facilitating further cluster growth, meaning that a greater amount of argon (higher pressure) leads to more collisions and, consequently, larger nanoparticles as observed in these experiments. Another possibility is that the Ni_5Ga_3 system deviates slightly from Thornton's model, which was developed from a different metal (Al, Cu vs Ni_5Ga_3), film thicknesses (>25 μm vs 50 nm), and deposition rates (>1000 Å/min vs 20 Å/min).

Other than synthesizing the films at considerable lower temperature, this method seems to favor the preferential growth of some crystal orientations: Figure 1c,d shows the growth of the (002) peak when normalized to the intensity of the (221) orientation peak. Also in this case, the evolution seems to stop at deposition pressures >15 mTorr, with a slight decrease in intensity for the (002) orientation of the film deposited at 20 mTorr. This preferential growth becomes even more pronounced when comparing these XRD results to those of a film postannealed at 385 °C in H_2 (Figure S5), which is known to be active for methanol synthesis.[5] It is evident that high-pressure depositions favor the (002) orientation, whereas the (221) and (402) orientations are more prevalent in postdeposition annealed films. Figures S6−S9 are different plots of the same XRD data to highlight the differences between samples. Such preferential growth of specific crystal orientations could be advantageous for catalytic applications, as catalytic activity can be correlated with different orientations. Thin films are also intriguing due to evident surface lattice strain compared to the simulated/expected δ-Ni_5Ga_3 diffraction pattern.[32] By varying the substrate, strain and stress effects could potentially be altered, introducing another parameter to consider when synthesizing catalysts and testing them for CO_2 hydrogenation. Synthesizing Ni_5Ga_3 films of the desired phase at room temperature, rather than at temperatures exceeding 600 °C (as required for chemical methods) or 385 °C (as shown in previous magnetron sputtering studies,[5] could be highly beneficial. This approach reduces energy consumption and production costs, making the synthesis process more sustainable and economically viable in view of a potential industrialization. Additionally, it allows for in situ characterizations immediately after deposition without the need of having a temperature control system in Ultra High Vacuum (UHV) analysis chambers. Lower temperature synthesis also makes this method more versatile for reactors that are temperature-sensitive and cannot withstand high temperatures due to design constraints.[33] Since Ni_5Ga_3 is used as a catalyst, it is important to check for the films' composition. Figures S10 and S11 show the survey spectrum and the fitted XPS Ni 2p/Ga 2p peaks to demonstrate the purity of the films and the expected Ni/Ga ratio on the surface of 5/3. Future studies

https://doi.org/10.1021/acsomega.4c08405
ACS Omega 2024, 9, 49759−49766

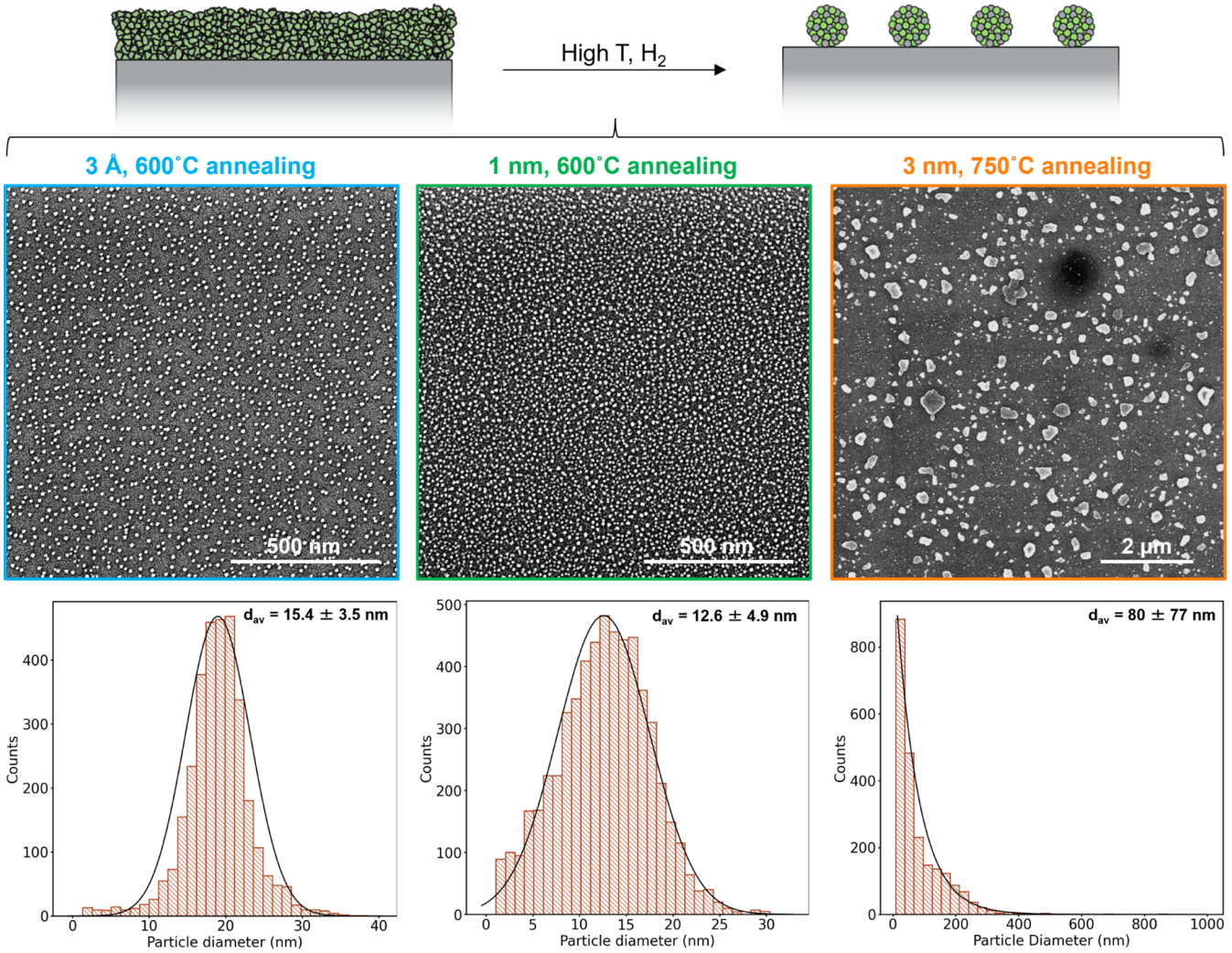

Figure 3. Annealing of ultrathin films to form nanoparticles. SEM image of different film thicknesses annealed at high temperature in H_2 and their particle size distribution.

could therefore focus on synthesizing and directly testing these films without air exposure for CO_2 hydrogenation to methanol. The interplay between deposition conditions and the resulting microstructure could be systematically explored to identify the optimal conditions for catalytic activity. These results could provide insights into the Ni_5Ga_3 active sites essential for methanol synthesis, potentially revealing the roles of surface facets, defects, and strain in catalytic performance.

Temperature is another essential parameter that can be modified during deposition. To investigate its effect on film growth, we varied the substrate temperature during the magnetron sputtering deposition process. The substrate was heated to specific temperatures during deposition to explore its influence on the crystallinity and microstructure of Ni_5Ga_3 films. The substrate temperature can facilitate atomic surface and bulk diffusion, potentially leading to increased grain size and the formation of different thermodynamically stable crystal phases. In this case, it becomes important not only to consider the Thornton model but also to examine the phase diagram for the Ni/Ga system.[34] As seen in Figure S2, the δ-phase appears unstable above 700 °C, leading instead to a two-phase region of α' and γ. Thin films of the same thickness (50 nm) were synthesized at different temperatures. Deposition pressures of 2 and 15 mTorr were chosen as the two extremes from the previous investigation. In Figure 2a,b, it is shown that when the substrate temperature is increased to 400 °C, XRD analysis reveals sharper and more intense diffraction peaks, indicating enhanced structural ordering and crystallite growth within the δ-Ni_5Ga_3 phase, especially for the thin films deposited at 2 mTorr. The grain size further increases at 600 °C, seemingly without significant influence from the pressure (Figure S8). This suggests that at this elevated temperature the thermal budget is sufficient to drive the crystallization process effectively regardless of the argon pressure, being predominantly controlled by bulk atomic diffusion rather than deposition pressure. At 800 °C, the deposited films appear to change to the more thermodynamically stable α' phase (with a crystal structure closer to that of Ni_3Ga_1), as expected from the phase diagram in Figure S2. Notably, the γ phase is absent in the XRD measurement, suggesting either the α' phase is possible at a Ni/Ga ratio of 5/3, contrary to the phase diagrams reported in the literature,[34] or that the excess Ga is present either in the bulk or on the surface as an amorphous phase, hence undetectable by XRD. An alternative possibility could be the sublimation of gallium within the sputter chamber during deposition. However, given that the sublimation temperature of gallium is higher at this pressure, this scenario is unlikely and was therefore ruled out. Interestingly, for

https://doi.org/10.1021/acsomega.4c08405
ACS Omega 2024, 9, 49759−49766

deposition at such high temperatures, pressure seems to become relevant again (Figure S8), with films deposited at 15 mTorr exhibiting much larger crystal sizes compared to those deposited at 2 mTorr. The difference in crystallinity is further evident when examining the shape and size of the crystals in both cases. Figure 2 shows that although the crystal phases at different temperatures are the same at both deposition pressures (2 and 15 mTorr), the crystal shape/film morphology is significantly different, with much larger grains forming at 15 mTorr, consistent with the previous findings on the deposition pressure influence at room temperature.

The results for the films deposited at 2 mTorr align closely with the Thornton model zones, exhibiting a gradual increase in crystal size with rising temperature. In contrast, for the 15 mTorr deposition, the influence of temperature is less pronounced, as the films already have relatively bigger crystal grains at room temperature. However, in this higher pressure case, temperature significantly impacts the shape of the crystals. Transitioning from 400 to 600 °C markedly affects the crystal grains' shape (Figure S12), suggesting that bulk diffusion becomes a key factor in film deposition. Therefore, deposition at 2 mTorr and temperatures above 600 °C likely falls into Zone T/Zone 2 of the model, characterized by surface diffusion, whereas deposition at 15 mTorr and temperatures above 600 °C likely falls into Zone 3, where growth is dominated by bulk diffusion. Figures S13−S20 present additional SEM images at various magnifications for all samples, emphasizing their differences and enabling direct comparison.

To further investigate the effect and potential of temperature, postgrowth annealing was also conducted to promote nanoparticles formation on selected samples. This annealing step, conducted in a hydrogen atmosphere, involved heating at 600 °C for 30 min after film growth. Nanoparticles are typically synthesized through chemical methods, which are popular due to their simplicity and low equipment cost. However, these methods require the effective removal of chemical precursors that can obscure the intrinsic catalytic activity and stability of the nanoparticles. This removal must be done without altering the nanoparticles' size, shape, or chemical state. Various strategies are employed for this purpose, including controlled thermal treatments under oxidizing and/or reducing atmospheres, UV light exposure, specific solvent washing treatments, and plasma treatments.[35−37] An alternative method involves using a cluster source for synthesizing well-defined and size-selected nanoparticles.[38,39] This technique offers significant advantages, especially in terms of size selection, composition, and cleanliness, as it avoids wet-chemistry.[39] However, it is costly and has low deposition rates (ranging between ng to μg/h). Nanoparticle formation on surfaces has been also studied through various techniques, including atomic layer deposition (ALD) and molecular beam epitaxy (MBE)[40,41] which offer precise control over nanoparticle size, distribution, and composition. Previous research has briefly shown that thin films of Ni_5Ga_3 can be annealed at high temperatures to form nanoparticles.[42,43] Given that those films annealed at 600 °C at various pressures exhibited comparable crystallinity of the desired δ-phase (Figure 2), applying the same treatment to ultrathin films deposited via magnetron sputtering is promising, following a similar approach of other thin film deposition techniques. The concept is to promote film dewetting and nanoparticle formation, a process driven by surface energy considerations, where thin layers tend to reorganize into isolated islands to minimize surface free energy.[40,41,44,45] This process depends on factors such as film thickness, deposition temperature, and substrate characteristics. The goal of this study is to leverage Ni/Ga dewetting to control the particle size of NiGa films, allowing for targeted morphological adjustments by tuning these parameters.

Figure 3 illustrates how annealing films of varying thicknesses under different temperature conditions influences the final particle size distribution, loading, and shape (see Figure S22 for the methodology). The 3 Å equivalent film shows the narrowest size distribution, with a final loading of about 19% projected area (Figure S23). In contrast, the 1 nm equivalent film has a slightly broader particle size distribution but a smaller average particle size, resulting in a higher particle density with approximately 34% loading (Figure S24). These two cases were analyzed also with Atomic Force Microscopy, which agrees with the relative difference in loading (projected coverage) and particle size distribution (Figures S25−S27). The 3 nm equivalent film thickness indicates a clear upper limit for achieving a uniform size selection. Since annealing this relatively thick film at 600 °C did not result in the full dewetting of the film (Figure S21), a temperature of 750 °C was used instead. Despite the higher annealing temperature to promote dewetting, the particles did not form uniformly, lacking homogeneity in surface distribution, size, and shape. The results can be compared with those shown by Sedano Varo et al.,[43] where films were annealed at 750 °C, again showing differences in the final particle size distribution (and likely crystal phase). Higher annealing temperatures affect both the average particle size and shape compared to annealing at 600 °C.

Synthesizing nanoparticles with this methodology offers several practical advantages. First, it becomes possible to *in situ* dewet the film into nanoparticles concurrent to the activation the catalyst. By adjusting the annealing time, different average particle sizes can be obtained and characterized from identical initial conditions. Making nanoparticles by exposing them to high temperatures causes them to reach their most stable point (if enough time is given), ensuring their stability under CO_2 hydrogenation reaction conditions, which typically occur around 250 °C, significantly lower than the annealing temperature of 600 °C.

To summarize, this study successfully demonstrates the synthesis of δ-Ni_5Ga_3 thin films at room temperature using magnetron sputtering, showing a temperature gap of approximately 350 °C compared to the previous study on the same catalyst via magnetron sputtering, and about 550 °C compared to other chemical synthesis methods. By systematically varying deposition pressure and temperature, the films exhibited significant improvements in crystal grain size. Higher deposition pressures, up to 20 mTorr, resulted in larger crystal grains, both at room temperature and up to 800 °C. The findings are consistent with the Thornton model, illustrating how deposition parameters such as pressure and temperature influence the final film morphology. This correlation provides deeper insights into the film growth process under different conditions. Moreover, ultrathin films were synthesized and annealed in H_2 at high temperatures, demonstrating the feasibility of producing size-controlled nanoparticles starting from films deposited through magnetron sputtering. Adjustments in the initial film thickness led to variations in particle size distribution, indicating that the fine-tuning of this

https://doi.org/10.1021/acsomega.4c08405
ACS Omega 2024, 9, 49759−49766

parameter can achieve the desired nanoparticle characteristics. The method can therefore be very versatile when considering all the other parameters that can be investigated, such as substrate material, substrate roughness, annealing temperature and time, and gas flow/composition.

In conclusion, magnetron sputtering proved to be a versatile and reproducible technique for the synthesis of thin films and nanoparticles. This makes it an effective method for studying catalyst properties in a controlled manner. This study underscores the effectiveness of magnetron sputtering for synthesizing high-quality δ-Ni_5Ga_3. It also exemplifies how to fully exploit the potential of magnetron sputtering as a technique to synthesize model system catalysts in various forms, paving the way for further research and development of other catalytic systems.

■ ASSOCIATED CONTENT

Supporting Information

The Supporting Information is available free of charge at https://pubs.acs.org/doi/10.1021/acsomega.4c08405.

Materials information; thin film preparation and handling after deposition; extra data and measurements of XRD, XPS, SEM, and AFM; literature synthesis comparison overview (PDF)

■ AUTHOR INFORMATION

Corresponding Authors

Filippo Romeggio − *DTU Physics, Technical University of Denmark, Kongens Lyngby DK-2800, Denmark;* orcid.org/0000-0001-6577-921X; Email: filro@dtu.dk

Christian D. Damsgaard − *DTU Physics and DTU Nanolab, Technical University of Denmark, Kongens Lyngby DK-2800, Denmark;* orcid.org/0000-0002-3117-8616; Email: cdda@dtu.dk

Authors

Rasmus Bischoff − *DTU Physics, Technical University of Denmark, Kongens Lyngby DK-2800, Denmark;* orcid.org/0009-0004-1499-3629

Clara B. Møller − *DTU Physics, Technical University of Denmark, Kongens Lyngby DK-2800, Denmark;* orcid.org/0009-0001-4175-4461

Victor L. Jensen − *DTU Physics, Technical University of Denmark, Kongens Lyngby DK-2800, Denmark*

Esteban Gioria − *DTU Physics, Technical University of Denmark, Kongens Lyngby DK-2800, Denmark;* orcid.org/0000-0001-6918-5734

Rikke Egeberg Tankard − *DTU Physics, Technical University of Denmark, Kongens Lyngby DK-2800, Denmark;* orcid.org/0000-0002-0060-642X

Rasmus S. Nielsen − *DTU Physics, Technical University of Denmark, Kongens Lyngby DK-2800, Denmark; Transport at Nanoscale Interfaces Laboratory, Swiss Federal Laboratories for Material Science and Technology (EMPA), Duebendorf 8600, Switzerland;* orcid.org/0000-0002-7600-9197

Ole Hansen − *DTU Nanolab, Technical University of Denmark, Kongens Lyngby DK-2800, Denmark;* orcid.org/0000-0002-6090-8323

Ib Chorkendorff − *DTU Physics, Technical University of Denmark, Kongens Lyngby DK-2800, Denmark;* orcid.org/0000-0003-2738-0325

Jakob Kibsgaard − *DTU Physics, Technical University of Denmark, Kongens Lyngby DK-2800, Denmark;* orcid.org/0000-0002-9219-816X

Complete contact information is available at: https://pubs.acs.org/10.1021/acsomega.4c08405

Author Contributions

#R.B., C.B.M., and V.L.J. contributed equally to this work. F.R.: investigation, methodology, formal analysis, writing−original draft, conceptualization. R.B.: investigation, writing−review and editing. C.B.M.: investigation, writing−review and editing. V.L.J.: investigation, writing−review and editing. E.G.G.: writing−review and editing, conceptualization. R.E.T.: investigation. R.S.N.: writing−review and editing, conceptualization. O.H.: writing−review and editing, supervision. I.C.: writing−review and editing, supervision. J.K.: writing−review and editing, supervision. C.D.D.: writing−review and editing, resources, conceptualization, supervision.

Funding

This work was supported by the European Union under the MSCA-Innovative Training Network Catchy (grant agreement no. 955650) and the European Research Council under the STORMING project (grant agreement no. 101069690).

Notes

The authors declare no competing financial interest.

■ ACKNOWLEDGMENTS

The authors are thankful for the funding from the EU Marie Skłodowska-Curie Actions-Innovative Training Network Catchy and from the European Research Council STORMING project.

■ REFERENCES

(1) Studt, F.; Sharafutdinov, I.; Abild-Pedersen, F.; Elkjær, C. F.; Hummelshøj, J. S.; Dahl, S.; Chorkendorff, I.; Nørskov, J. K. Discovery of a Ni-Ga catalyst for carbon dioxide reduction to methanol. *Nat. Chem.* **2014**, *6* (4), 320−324.

(2) Sharafutdinov, I.; Elkjær, C. F.; De Carvalho, H. W. P.; Gardini, D.; Chiarello, G. L.; Damsgaard, C. D.; Wagner, J. B.; Grunwaldt, J. D.; Dahl, S.; Chorkendorff, I. Intermetallic compounds of Ni and Ga as catalysts for the synthesis of methanol. *J. Catal.* **2014**, *320* (1), 77−88.

(3) Gallo, A.; Snider, J. L.; Sokaras, D.; Nordlund, D.; Kroll, T.; Ogasawara, H.; Kovarik, L.; Duyar, M. S.; Jaramillo, T. F. Ni5Ga3 catalysts for CO2 reduction to methanol: Exploring the role of Ga surface oxidation/reduction on catalytic activity. *Appl. Catal., B* **2020**, *267*, 118369.

(4) Zimmerli, N. K.; Rochlitz, L.; Checchia, S.; Müller, C. R.; Copéret, C.; Abdala, P. M. Structure and Role of a Ga-Promoter in Ni-Based Catalysts for the Selective Hydrogenation of CO2 to Methanol. *JACS Au* **2024**, *4* (1), 237−252.

(5) Romeggio, F.; Schouenborg, J. F.; Vesborg, P. C. K.; Hansen, O.; Kibsgaard, J.; Chorkendorff, I.; Damsgaard, C. D. Magnetron Sputtering of Pure δ-Ni5Ga3 Thin Films for CO2 Hydrogenation. *ACS Catal.* **2024**, *14*, 12592−12601.

(6) Chen, P.; Zhao, G.; Liu, Y.; Lu, Y. Monolithic Ni5Ga3/SiO2/Al2O3/Al-fiber catalyst for CO2 hydrogenation to methanol at ambient pressure. *Appl. Catal., A* **2018**, *562*, 234−240.

(7) Nguyen, H. K. D.; Dang, T. H. Conversion of CO2 to methanol using NiGa/mesosilica (NiGa/MSO) catalyst. *J. Porous Mater.* **2019**, *26* (5), 1297−1304.

(8) Ahmad, K.; Upadhyayula, S. Conversion of the greenhouse gas CO2 to methanol over supported intermetallic Ga-Ni catalysts at atmospheric pressure: Thermodynamic modeling and experimental study. *Sustainable Energy Fuels* **2019**, *3* (9), 2509−2520.

(9) Nguyen, H. K. D.; Dang, T. H.; Dinh, N. T.; Duy Nguyen, H. H. Study on characterization and application of novel Ni-Ga based catalysts in conversion of carbon dioxide to methanol. *AIP Adv.* **2019**, *9*, 085006.
(10) Goyal, R.; Lee, J.; Sameer, S.; Sarkar, B.; Chiang, K.; Bordoloi, A. CNx stabilized Ni-Ga nanoparticles for CO 2 hydrogenation: Role of preparation methods. *Catal. Today* **2020**, *343*, 48−55.
(11) Men, Y.; Fang, X.; Gu, Q.; Singh, R.; Wu, F.; Danaci, D.; Zhao, Q.; Xiao, P.; Webley, P. A. Synthesis of Ni5Ga3 catalyst by Hydrotalcite-like compound (HTlc) precursors for CO2 hydrogenation to methanol. *Appl. Catal., B* **2020**, *275*, 119067.
(12) Duyar, M. S.; Gallo, A.; Snider, J. L.; Jaramillo, T. F. Low-pressure methanol synthesis from CO2 over metal-promoted Ni-Ga intermetallic catalysts. *J. CO2 Util.* **2020**, *39*, 101151.
(13) Ahmad, K.; Anushree; Upadhyayula, S. Deactivation behaviour of intermetallic Ga-Ni catalyst in CO2 hydrogenation to methanol. *Greenhouse Gases: Sci. Technol.* **2021**, *11* (5), 1056−1065.
(14) Rasteiro, L. F.; De Sousa, R. A.; Vieira, L. H.; Ocampo-Restrepo, V. K.; Verga, L. G.; Assaf, J. M.; Da Silva, J. L. F.; Assaf, E. M. Insights into the alloy-support synergistic effects for the CO 2 hydrogenation towards methanol on oxide-supported Ni 5 Ga 3 catalysts: An experimental and DFT study. *Appl. Catal., B* **2022**, *302*, 120842.
(15) Proaño, L.; Jones, C. W. CO2 hydrogenation to methanol over ceria-zirconia NiGa alloy catalysts. *Appl. Catal., A* **2024**, *669*, 119485.
(16) Chiang, C. L.; Lin, K. S.; Lin, Y. G. Preparation and Characterization of Ni5Ga3 for Methanol Formation via CO2 Hydrogenation. *Top. Catal.* **2017**, *60* (9−11), 685−696.
(17) Ahmad, K.; Upadhyayula, S. Selective conversion of CO 2 to methanol over intermetallic Ga-Ni catalyst: Microkinetic modeling. *Fuel* **2020**, *278*, 118296.
(18) Cortés-Reyes, M.; Azaoum, I.; Molina-Ramírez, S.; Herrera, C.; Larrubia, M. Á.; Alemany, L. J. NiGa Unsupported Catalyst for CO2 Hydrogenation at Atmospheric Pressure. Tentative Reaction Pathways. *Ind. Eng. Chem. Res.* **2021**, *60* (51), 18891−18899.
(19) Rasteiro, L. F.; Rossi, M. A. L. S.; Assaf, J. M.; Assaf, E. M. Low-pressure hydrogenation of CO2 to methanol over Ni-Ga alloys synthesized by a surfactant-assisted co-precipitation method and a proposed mechanism by DRIFTS analysis. *Catal. Today* **2021**, *381*, 261−271.
(20) Lin, K. S.; Hussain, A.; Lin, Y. S.; Hsieh, Y. C.; Chiang, C. L. Direct synthesis of CH3OH from CO2 hydrogenation over Ni5Ga3/SiO2 catalysts. *Fuel* **2023**, *348*, 128504.
(21) Nguyen, H. K. D.; Dang, T. H.; Nguyen, N. L. T.; Nguyen, H. T.; Dinh, N. T. Novel Ni-Ga Alloy Based Catalyst for Converting CO 2 to Methanol. *Can. J. Chem. Eng.* **2017**, *96*, 832−837.
(22) Hejral, U.; Timoshenko, J.; Kordus, D.; Lopez Luna, M.; Divins, N. J.; Widrinna, S.; Zegkinoglou, I.; Pielsticker, L.; Mistry, H.; Boscoboinik, J. A.; Kuehl, S.; Roldan Cuenya, B. Tracking the phase changes in micelle-based NiGa nanocatalysts for methanol synthesis under activation and working conditions. *J. Catal.* **2022**, *405*, 183−198.
(23) Zhou, H.; Zhang, S.; Shao, Y.; Liu, S.; Fan, X.; Chen, H. Relationship between Structural Properties of the Unsupported Ni5Ga3 Catalyst and Methanol Synthesis Activity. *Ind. Eng. Chem. Res.* **2024**, *63*, 6984.
(24) Tankard, R. E.; Romeggio, F.; Akazawa, S. K.; Krabbe, A.; Sloth, O. F.; Secher, N. M.; Colding-Fagerholt, S.; Helveg, S.; Palmer, R.; Damsgaard, C. D.; Kibsgaard, J.; et al. Stable mass-selected AuTiOx nanoparticles for CO oxidation. *Phys. Chem. Chem. Phys.* **2024**, *26*, 9253−9263.
(25) Thornton, J. A. *Sputter Coating- Its Principles And Potential On JSTOR*. 1973. https://www.jstor.org/stable/44717585.
(26) Thornton, J. A. Influence of apparatus geometry and deposition conditions on the structure and topography of thick sputtered coatings. *J. Vac. Sci. Technol.* **1974**, *11* (4), 666−670.
(27) Thornton, J. A. Influence of substrate temperature and deposition rate on structure of thick sputtered Cu coatings. *J. Vac. Sci. Technol.* **1975**, *12* (4), 830−835.
(28) Thornton, J. A. High Rate Thick Film Growth. *Annu. Rev. Mater. Sci.* **1977**, *7* (1), 239−260.
(29) Haberland, H.; Karrais, M.; Mall, M.; Thurner, Y. Thin films from energetic cluster impact: A feasibility study. *J. Vac. Sci. Technol., A* **1992**, *10* (5), 3266−3271.
(30) Goldby, I. M.; Von Issendorff, B.; Kuipers, L.; Palmer, R. E. Gas condensation source for production and deposition of size-selected metal clusters. *Rev. Sci. Instrum.* **1997**, *68* (9), 3327−3334.
(31) Popok, V. N.; Barke, I.; Campbell, E. E. B.; Meiwes-Broer, K. H. Cluster-surface interaction: From soft landing to implantation. *Surf. Sci. Rep.* **2011**, *66* (10), 347−377.
(32) Jain, A.; Ong, S. P.; Hautier, G.; Chen, W.; Richards, W. D.; Dacek, S.; Cholia, S.; Gunter, D.; Skinner, D.; Ceder, G.; Persson, K. A. Commentary: The materials project: A materials genome approach to accelerating materials innovation. *APL Mater.* **2013**, *1* (1), 11002.
(33) Abbas, I.; Romeggio, F.; Pilarczyk, K.; Kuhn, S.; Damsgaard, C. D.; Kibsgaard, J.; Lievens, P.; Grandjean, D.; Janssens, E.; High pressure microreactor for minute amounts of catalyst on planar supports: A case study of CO2 hydrogenation over Pd0.25Zn0.75Ox nanoclusters. *Chem. Eng. J.* **2024**, 158127 .
(34) Ducher, R.; Kainuma, R.; Ishida, K. Phase equilibria in the Ni-rich portion of the Ni-Ga binary system. *Intermetallics* **2007**, *15* (2), 148−153.
(35) Cargnello, M.; Chen, C.; Diroll, B. T.; Doan-Nguyen, V. V. T.; Gorte, R. J.; Murray, C. B. Efficient removal of organic ligands from supported nanocrystals by fast thermal annealing enables catalytic studies on well-defined active phases. *J. Am. Chem. Soc.* **2015**, *137* (21), 6906−6911.
(36) Gioria, E.; Li, S.; Mazheika, A.; Naumann d'Alnoncourt, R.; Thomas, A.; Rosowski, F. CuNi Nanoalloys with Tunable Composition and Oxygen Defects for the Enhancement of the Oxygen Evolution Reaction**. *Angew. Chem., Int. Ed.* **2023**, *62* (26), 202217888.
(37) Cuenya, B. R. Metal nanoparticle catalysts beginning to shape-up. *Acc. Chem. Res.* **2013**, *46* (8), 1682−1691.
(38) Pratontep, S.; Carroll, S. J.; Xirouchaki, C.; Streun, M.; Palmer, R. E. Size-selected cluster beam source based on radio frequency magnetron plasma sputtering and gas condensation. *Rev. Sci. Instrum.* **2005**, *76* (4), 045103.
(39) Grammatikopoulos, P.; Steinhauer, S.; Vernieres, J.; Singh, V.; Sowwan, M. Nanoparticle design by gas-phase synthesis. *Adv. Phys.: X* **2016**, *1* (1), 81−100.
(40) Richey, N. E.; De Paula, C.; Bent, S. F. Understanding chemical and physical mechanisms in atomic layer deposition. *J. Chem. Phys.* **2020**, *152* (4), 040902.
(41) Aouassa, M.; Bouabdellaoui, M.; Yahyaoui, M.; Kallel, T.; Ettaghzouti, T.; Algarni, S. A.; Althobaiti, I. O. Mn-Doped Ge Nanoparticles Grown on SiO2Thin Films by Molecular Beam Epitaxy for Photodetector and Solar Cell Applications. *ACS Appl. Electron. Mater.* **2023**, *5* (5), 2696−2703.
(42) Damsgaard, C. D.; Duchstein, L. D. L.; Sharafutdinov, I.; Nielsen, M. G.; Chorkendorff, I.; Wagner, J. B. In situ ETEM synthesis of NiGa alloy nanoparticles from nitrate salt solution. *Microscopy* **2014**, *63*, 397−401.
(43) Sedano Varo, E.; Tankard, R. E.; Needham, J. L.; Gioria, E.; Romeggio, F.; Chorkendorff, I.; Damsgaard, C. D.; Kibsgaard, J. An experimental perspective on nanoparticle electrochemistry. *Phys. Chem. Chem. Phys.* **2024**, *26* (25), 17456−17466.
(44) Andalouci, A.; Brinza, O.; Porosnicu, C.; Lungu, C.; Mazaleyrat, F.; Roussigné, Y.; Chérif, S. M.; Farhat, S. Morphological and magnetic study of plasma assisted solid-state dewetting of ultra-thin cobalt films on conductive titanium silicon nitride supports. *Thin Solid Films* **2020**, *703*, 137973.
(45) Sonawane, D.; Choudhury, A.; Kumar, P. New Insights into Dewetting of Cu Thin Films Deposited on Si. *Langmuir* **2020**, *36* (20), 5534−5545.

https://doi.org/10.1021/acsomega.4c08405
ACS Omega 2024, 9, 49759−49766